

ISSN: (Print) (Online) Journal homepage: <https://www.tandfonline.com/loi/tbsd20>

Development of novel chromones as antioxidant COX2 inhibitors: *in vitro*, QSAR, DFT, molecular docking, and molecular dynamics studies

Arunapriya Lakkadi, Srimai Vuppala, Venkatesh Nampally, Jaeyoung Kim, Kiduk Kim, Joonkyung Jang & Parthasarathy Tigulla

To cite this article: Arunapriya Lakkadi, Srimai Vuppala, Venkatesh Nampally, Jaeyoung Kim, Kiduk Kim, Joonkyung Jang & Parthasarathy Tigulla (2023): Development of novel chromones as antioxidant COX2 inhibitors: *in vitro*, QSAR, DFT, molecular docking, and molecular dynamics studies, Journal of Biomolecular Structure and Dynamics, DOI: [10.1080/07391102.2023.2212785](https://doi.org/10.1080/07391102.2023.2212785)

To link to this article: <https://doi.org/10.1080/07391102.2023.2212785>



View supplementary material [↗](#)



Published online: 15 May 2023.



Submit your article to this journal [↗](#)



View related articles [↗](#)



View Crossmark data [↗](#)



Development of novel chromones as antioxidant COX2 inhibitors: *in vitro*, QSAR, DFT, molecular docking, and molecular dynamics studies

Arunapriya Lakkadi^{a*}, Srimai Vuppala^{b*}, Venkatesh Nampally^c, Jaeyoung Kim^b, Kiduk Kim^b, Joonkyung Jang^b and Parthasarathy Tigulla^c

^aDepartment of Chemistry, Bhavan's Vivekananda College of Science, Humanities & Commerce, Sainikpuri, Secunderabad, India;

^bDepartment of Nanoenergy Engineering, Pusan National University, Busan, Republic of Korea; ^cDepartment of Chemistry, Osmania University, Hyderabad, India

Communicated by Ramaswamy H. Sarma

ABSTRACT

The chromone derivatives are playing a prominent role in many plant cycles, for instance, the regulation of growth, stimulation of oxygen uptake in plants, and essential food constituents with valuable pro-health properties. Determination of the antioxidant activity of these compounds is an interesting approach to drug design and development. The antioxidant activity of the novel fifteen chromone compounds was estimated by using a spectrophotometric Dichloro-5,6-dicyano 1,4-benzoquinone (DDQ) assay method and the mechanism of antioxidant activity was discussed based on the Density functional theory (DFT) calculations. The compounds showed significant antioxidant activity which was correlated to their molecular structure by considering various molecular descriptors. Further, by using regression analysis QSAR-modeled equation was proposed and it has shown a high correlation coefficient value (0.946). We perform molecular docking and molecular dynamics simulations against the cyclooxygenase (COX2) enzyme to investigate the molecule's anti-inflammatory activity and stability of protein-ligand complexes. Molecular docking and dynamics simulations revealed the compounds B3 and B8 were interacting with essential residues TYR385, HIS386, ASN382, TRP387, and HIS388 in the binding site that were crucial for optimizing heme and the resultant peroxidase and cyclooxygenase activities. The root mean square displacement and root mean square fluctuation plots revealed the stability of the B3-COX2 and B8-COX2 complexes. Based on our results, B3 and B8 compounds are considered as best antioxidants as well as COX2 inhibitors.

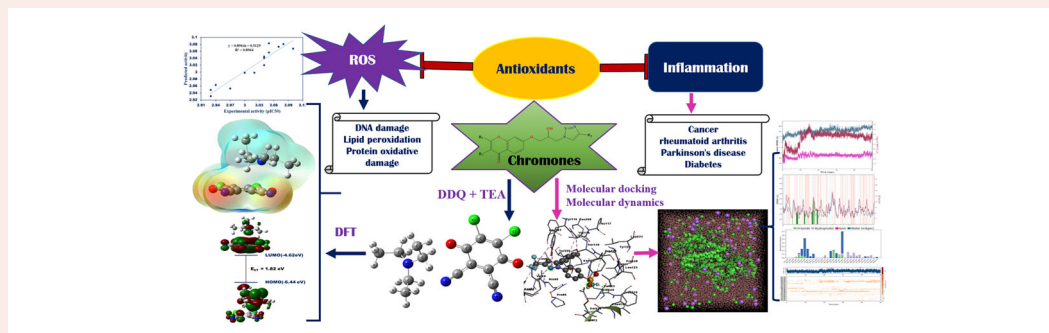
ARTICLE HISTORY

Received 19 January 2023

Accepted 20 April 2023

KEYWORDS





Antioxidants; COX2 inhibitors; *in vitro*; QSAR; molecular docking; molecular dynamics; DFT




1. Introduction

Free radicals are endlessly produced in the human cellular metabolism in the form of reactive oxygen species (ROS) and reactive nitrogen species (RNS) and these species can damage normal tissues and biomolecules such as proteins, DNA, and lipid membranes (Halliwell & Gutteridge, 2015; Kruk, 1997; Termini, 2000; Valko et al., 2007). However, the cellular system is also well-resourced with an efficient free radical

scavenging (antioxidant) system that is mainly composed of both enzymatic (superoxide dismutase, lipid peroxidase, and catalase) and non-enzymatic (vitamin C, glutathione, and uric acid) molecules that can maintain the adverse effects of these free radicals (Alam et al., 2013). During diseases or under stressful conditions, the cell's antioxidant production decreases, which increases the ROS/antioxidant ratio, which is called oxidative stress (Pizzino et al., 2017). Oxidative stress (lipid peroxidation) is a major cause of many pathological

CONTACT Joonkyung Jang  jkjang@pusan.ac.kr  Department of Nanoenergy Engineering, Pusan National University, Busan 46241, Republic of Korea; Parthasarathy Tigulla  sarathychem@gmail.com  Department of Chemistry, Osmania University, Hyderabad 500007, India.

*These authors have contributed equally to this work and share the first authorship.

 Supplemental data for this article can be accessed online at <https://doi.org/10.1080/07391102.2023.2212785>.

© 2023 Informa UK Limited, trading as Taylor & Francis Group

diseases such as neurodegenerative disorders like Alzheimer's, inflammation, diabetes, liver disorders, hypertension, and rheumatoid arthritis (De Vries, 2006; Fu et al., 1990; Hawkey, 2005; Pizzino et al., 2017). According to the review, the author Markus Laube et al. (2016) reported that as a result of ROS-mediated stimulation of a cascade of enzymes such as Phospholipase A2, transcription factors such as nuclear factor kappa B pathways, E2 promoter binding factor-1, hypoxia-inducible factor 2α , and the radiation therapy induces extreme production of cyclooxygenases (COXs)-mediated eicosanoids (prostaglandins and thromboxane).

COXs are also known as Prostaglandin-endoperoxide H synthases (PGHSs), which are rate-limiting enzymes for the conversion of arachidonic acid to prostaglandins, two molecules of O_2 , and two electrons to prostaglandin endoperoxide H_2 (PGH₂). In order to form PGH₂, arachidonate is first oxygenated to yield prostaglandin G2 (PGG2) using the enzyme's cyclooxygenase activity, and then the 15-hydroperoxyl group of PGG2 is reduced to produce PGH₂ using the enzyme's peroxidase. PGHSs exist in two isoforms, PGHS-1 (COX1) is a constitutive enzyme, whereas PGHS-2 (COX2) is the inducible isoform (Kujubu et al., 1991; Marnett et al., 1999; Smith et al., 2000; Xie & Herschman, 1996). Inflammatory sites are primarily affected by COX2, responsible for the induced production of prostaglandins. There is substantial evidence suggesting that COX2 overexpression is associated with chronic inflammatory diseases such as rheumatoid arthritis, neurodegenerative disorders such as Parkinson's disease, as well as a wide range of cancers (De Vries, 2006; Fu et al., 1990; Hawkey, 2005). This enzyme exhibits several unique properties that make it an interesting and drug-able target (Laube et al., 2013). Our work mainly aims to substantiate the development of novel chromone compounds as antioxidant COX2 inhibitors. Chromones are naturally occurring secondary metabolites, especially in the plant kingdom which are oxygen-containing heterocyclic compounds. Recent reviews and research articles reported that chromone is a core moiety of natural products such as flavonoids, isoflavonoids, and polyphenols which exerts antioxidant (Preeti et al., 2014), anti-inflammatory, anti-arthritis, anti-cancer, and anti-allergic activities (Reis et al., 2017). Chromones inhibit various mechanisms, including COX1 and COX2 enzymes, and NO synthesis, which are responsible for their anti-inflammatory effects. Several naturally occurring chromones have anti-inflammatory properties, including nor-cimicifugin, eugenin, petersinone 1, stellatin, and aloesin (Gamal-Eldeen et al., 2007; Gautam et al., 2010; Yagi et al., 2002). In addition, chromones can scavenge many types of ROS and inhibit lipid peroxidation (Laube et al., 2016). In this regard, we calculated the free radical scavenging activity of novel chromone derivatives (Bandari et al., 2017; Bandari & Kommu, 2016) (Figure 1) against 2,3-Dichloro-5,6-dicyano-1,4-benzoquinone (DDQ) (Rao et al., 1972) and performed in silico analysis to explore the anti-inflammatory activity. The DDQ assay method utilizes the concept of charge transfer (CT) complex phenomena in between donor-acceptor and the stability of CT complex discussed with theoretical density functional theory (DFT) calculations. Scavenging of free

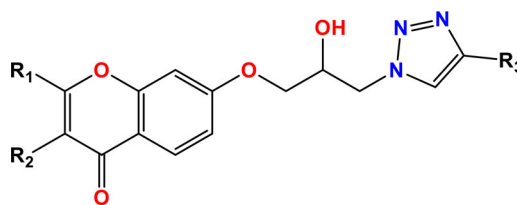


Figure 1. Molecular structure of chromone derivatives.

radicals can be accomplished through rapid hydrogen transfer. In this regard, an antioxidant capacity of a compound is influenced greatly by several factors such as the arrangement or substitution pattern of functional groups and the number of donating or withdrawing groups present in the molecules. A small change in the above-listed factors can significantly influence the physicochemical and biological properties of the molecules. Therefore, in this paper, we calculated the Quantitative structure-activity relationship (QSAR) to correlate the molecular descriptors with their estimated antioxidant activity. The DFT method was utilized to calculate the molecular descriptors of chromones.

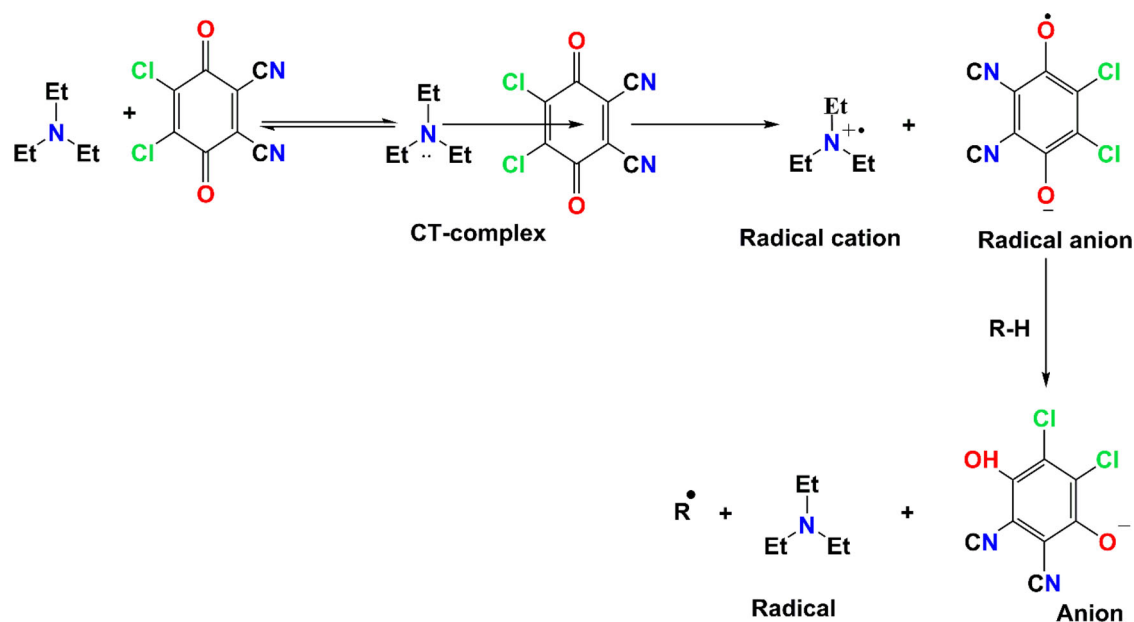
In this study, molecular docking and molecular dynamics (MD) simulations are performed to explore the inhibitory activity of chromones against the COX2 target (Amira et al., 2022; Jones Lipinski et al., 2021). Molecular docking and MD simulations are powerful computational methods in the drug design and discovery process. The MD simulations may provide information about the inhibitor's key interactions and structure-dynamic characteristics at the molecular level of COX2's binding site. Ultimately, the work will contribute to the development of more potent COX2 inhibitors through structure-based drug discovery.

2. Materials and methods

The materials DDQ (98%), triethyl amine (TEA; 99%), and acetonitrile (98%) are purchased from Sigma Aldrich online sources. UV-Visible absorption spectra were analyzed in the nanometer region using SHIMADZU UV-2600 and UV-VIS spectrophotometer. The main reaction scheme and synthesis procedure for selected chromone derivatives were published in our previous report (Bandari et al., 2017; Bandari & Kommu, 2016) and the synthesis reaction scheme (Scheme S1) is also provided in the supplementary data.

2.1. Evaluation of antioxidant activity

The standard solution of the donor (TEA) 0.72 M was prepared by dissolving 0.726 g (0.726 g/cc) in acetonitrile in a 10 ml volumetric flask. From the above standard solution, 5.0×10^{-4} mol. L⁻¹ was created in a separate volumetric flask by diluting the solution with the same acetonitrile solvent. The standard stock solution of the acceptor (DDQ) is 10^{-2} mol. L⁻¹ was produced by dissolving 0.023 g in acetonitrile solvent in a 10 ml standard flask, and the same solution was diluted to 5.0×10^{-4} mol. L⁻¹ in a 25 ml standard flask using acetonitrile solvent. Necessary arrangements were made to protect the produced stock solutions of TEA and



Scheme 1. Mechanism of CT Complex formation with the acceptor (DDQ) and donor (TEA).

DDQ from direct light. By mixing equal molar concentration of 5.0×10^{-4} mol. L^{-1} in the ratio 1:1 between TEA and DDQ in acetonitrile solvent a reddish-brown color was obtained as CT complex. The molar concentration of 10^{-5} mol. L^{-1} chromone compounds was added into test tubes and dissolved in acetonitrile to obtain a series of solutions. Then, 2 ml of CT complex solution was added to each tube containing 1 ml of solution, stirred, and allowed to rest/stand for 5 min at room temperature. The maximum absorbance of the final mixture was measured at 450 nm and ascorbic acid was considered as the standard/control sample to calculate the radical scavenging activity of the test compounds. The radical scavenging activity of DDQ was calculated using the following equation.

$$\% \text{ Radical Scavenging Activity } (R_s) = \frac{A_b - A_a}{A_b} \times 100$$

where A_b = Initial absorbance of the CT complex and A_a = Absorbance of the test/standard compound.

The antioxidant activity of the compounds was expressed in IC_{50} which means the concentration of the test compound inhibits 50% of the DDQ radicals.

2.2. Computational details

The molecular structures of chromone compounds, DDQ, TEA, and CT complex were constructed and the energy minimization was carried out using Gaussian 16 program (Frisch et al., 2016). The Becke–Lee–Yang–Parr hybrid exchange–correlation three-parameter functional (B3LYP) and basis set 6-31 G(d) (Becke, 1993, 1996) was employed to optimize the molecular structures and to compute the vibrational frequencies of chromones. The Berny optimization algorithm is a standard algorithm used to optimize molecular structures by minimizing the potential energy surface. Vibrational frequencies can provide valuable information about the molecular structure, such as bond lengths and bond angles. This

algorithm iteratively adjusts the atomic positions until local minima are found. We performed the population analysis to unveil the electron density distributions of the frontier molecular orbitals. The geometrical parameters of the CT complex such as bond lengths, bond angles, highest occupied molecular orbital (HOMO), lowest unoccupied molecular orbital (LUMO) isodensity surfaces, and molecular electrostatic potential (MEP) map of the CT complex were calculated by using the same level of theory. Molecular descriptors viz, ionization potential (IP), electron affinity (EA), hardness (η), HOMO, LUMO, polarizability (POL), dipole moment (DM), chemical potential (μ), entropy (S), electrophilic index (ω), and heat capacity (Cv) of chromone compounds were calculated using DFT method. To correlate the experimental activity with molecular descriptors of the compounds, regression analysis was carried out using SPSS10 software (n.d.). In the Molinspiration tool (<http://www.molinspiration.com/>), partition coefficient (LogP) and enzyme inhibitor score (EI) were calculated to understand the nature (hydrophilic/hydrophobic) of chromone derivatives and their antioxidant potential.

In order to calculate η , μ , and ω , we calculated the ionization potential and electron affinity using the following equations.

$$\begin{aligned}
 IP &= -E_{\text{HOMO}} \\
 EA &= -E_{\text{LUMO}} \\
 \eta &= IP - EA/2 \\
 \mu &= -EA - IP/2 \\
 \omega &= \mu^2/2\eta
 \end{aligned}$$

2.3. Molecular docking simulations

To develop novel chromones as antioxidant COX2 inhibitors, the most efficient computer-aided drug design technique molecular docking was utilized. The X-ray crystallographic

structure of the target enzyme COX2 was retrieved from the RCSB protein data bank with a PDB code of 4COX (Amira et al., 2022; Jones Lipinski et al., 2021). The molecular docking studies were performed with two well-known docking programs such as Genetic Optimization for Ligand Docking (GOLD) (Jones et al., 1997) and AutoDock 4.2 (Morris et al., 2008) tool. The GOLD program uses a genetic algorithm to search the best-fit positions and orientations of the ligand within the binding site. One of the key features of GOLD is its ability to account for ligand conformational flexibility during the docking process. In other words, the GOLD can explore multiple possible conformations of the ligand and evaluate their fit within the binding site, rather than assuming a fixed conformation. In addition, it allows for partial flexibility of the protein, which means certain parts of the protein binding site can move slightly to accommodate the ligand during the docking process. We prepared the protein using the method described by Jones et al. (1997), in which, the water molecules and hetero atoms were removed, then hydrogen atoms were added according to protonation states. After preparing the protein, the molecular structures of all ligands were also prepared and energetically minimized using Gaussian 16 program. The GOLD program requires that the user select the protein-ligand interaction distance and active site radius, then we set these parameters as 1.5 and 10 Å (Srimai et al., 2013), respectively, and the other parameters such as population size of 100 and selection pressure of 1.1 were fixed to default values. We used the GOLD program to evaluate two scoring functions: Fitness score, which measures the geometric fit of the ligand in the binding site, and Chem score, which estimates the intermolecular interactions between the ligand and the receptor.

AutoDock tool provides a user-friendly graphical interface for performing tasks such as the creation of ligand and protein files, adding hydrogens, assigning charges, and generating grid maps for docking simulations. The protein structure was typically prepared by removing water molecules and any other non-protein components, adding hydrogen atoms to the structure, and assigning partial charges to the atoms. All the ligands were prepared by adding Gasteiger charges and the maximum number of torsions were set as 5 and saved as pdbqt files. A grid map is generated around the protein to define the search space for docking simulations. This involves defining the center of the grid and the spacing between the grid points. During the docking simulation, the ligand is moved around the search space defined by the grid map, and the energy of the ligand-protein complex is calculated for each position. The results of the docking simulation were analyzed to identify the binding site of the ligand and to rank the binding poses based on the calculated energy.

2.4. Molecular dynamics simulations

As a result of molecular docking, the best two protein-ligand complexes (lowest binding energy and highest fitness score) are analyzed for their stability and dynamics under solvent conditions using molecular dynamics simulations. Desmond in Schrodinger suite v2022-1 (Bergdorf et al., 2021; Bowers

et al., 2006) was utilized to perform the MD simulations of the protein-ligand complexes. Using a 'system builder' module, the predefined TIP3P water model is filled in an orthorhombic box along with a buffer at a distance of 10 Å from the box edge to the center. The periodic boundary condition box volume was calculated as per complex type along with the counter ions Na^+/Cl^- were added to neutralize the protein-ligand systems. OPLS_2005 force field parameters were used to minimize the solvated systems. To restrain heavy atoms on the solute, the Berendsen NVT ensemble was used to simulate the system. Under isothermal isobaric conditions and a thermostat relaxation time of 100 ps, MD simulations were carried out with a temperature of 300K, and a pressure of 1 atm. The Nose-Hoover thermostat and Martyna-Tobias-Klein barostat approaches have been employed for MD simulations in order to maintain 300K and 1 atm temperature and pressure. The NPT ensemble was initiated following the simulation process which runs for 50 ns production. For every 5 picoseconds, the simulation progress was recorded step by step.

3. Results and discussion

3.1. The free radical scavenging activity of chromone compounds

The radical scavenging activity of fifteen chromone compounds (Table 1) was calculated by using the DDQ assay method. The method utilizes the concept of a CT complex between the electron donor and acceptor which absorbs radiation at the visible region (Brame & Dekker, 1972; Foster, 1969). The absorbance of novel chromone compounds was calculated using a UV-visible spectrophotometer. It is a well-known fact that the DDQ and TEA act as good π -electron acceptors and donors, respectively, and form a stable and highly intense colored CT complex (Salem, 2002). The reaction mechanism involved in the CT complex formation of DDQ-TEA was explained in Scheme 1. It represents the formation of the CT complex followed by the DDQ radical anion. The odd electron which is present on DDQ abstracts H-atom from an antioxidant (chromones). The CT complex which was obtained by the interaction between the donor

Table 1. Free radical scavenging activity of chromone compounds and standard ascorbic acid.

Compounds	R1	R2	R3	%RS	IC ₅₀ (mM)	Activity (mM)
B1	H	CH3	-C6H5	55.90	0.890	3.05
B2	H	CH3	-pC6H4CH3	55.11	0.907	3.04
B3	H	CH3	-pC6H4OCH3	59.84	0.830	3.08
B4	H	CH3	-pC6H4C2H5	51.18	0.976	3.01
B5	H	CH3	-mC6H4NH2	50.39	0.992	3.00
B6	CH3	CH3	-C6H5	55.90	0.890	3.05
B7	CH3	CH3	-pC6H4CH3	34.09	1.466	2.83
B8	CH3	CH3	-pC6H4OCH3	62.90	0.794	3.10
B9	CH3	CH3	-pC6H4C2H5	54.54	0.916	3.04
B10	CH3	CH3	-pC6H4NH2	42.50	1.174	2.93
B11	CH3	-C6H5	-C6H5	52.27	0.956	3.02
B12	CH3	-C6H5	-pC6H4CH3	45.45	1.100	2.93
B13	CH3	-C6H5	-pC6H4OCH3	43.93	1.138	2.94
B14	CH3	-C6H5	-pC6H4C2H5	46.82	1.061	2.97
B15	CH3	-C6H5	-mC6H4NH2	58.73	0.850	3.07
Ascorbic Acid				45.60	1.096	2.96

and acceptor will act as a source of free radicals. Out of these 15 compounds, 11 compounds have exhibited high scavenging activity compared to that of standard ascorbic acid. The compounds B8, B3, and B15 have shown significant antioxidant activity with IC₅₀ values of 0.794 mM, 0.830 mM, and 0.850 mM, respectively.

3.2. Interpretation of CT complex formation with theoretical DFT studies

3.2.1. Estimation of bond lengths and bond angles

To explain the CT complex formation between donor and acceptor, theoretically, we optimize the geometries of TEA, DDQ, and TEA-DDQ CT complex by using DFT calculations. The change in bond lengths of C-O in optimized geometries of DDQ and CT complex confirms the electron transfer from TEA to DDQ (acceptor) (Arunapriya et al., 2017; Nampally et al., 2022; Venkatesh et al., 2019). In DDQ, the bond length of C-O (C2=O8 and C5=O8) increased from 1.213 Å to 1.216 Å (C23=O30) and 1.215 Å (C26=O29) in the CT complex. Furthermore, we observed the changes in bond lengths of optimized geometries of TEA isolated and the complex. A bond length of 1.468 Å is changed to 1.475, 1.468, and 1.474 Å for each of the three N-C bonds (N1-C2, N1-C9, and N1-C16). The CT complex formation in between DDQ and TEA can also be confirmed by the change in bond angles of DDQ alone and CT complex. Two bond angles with values of each 117.274°, such as C24-C23-C28 and C25-C26-C27, were changed to 117.037° and 116.99°, respectively.

3.2.2. Molecular electrostatic potential surface maps (MEPs)

In order to electrophilic and nucleophilic centers in a molecule, MEPs are the most appropriate graphical representations. The MEPs were calculated from the optimized geometries of the TEA, DDQ, and CT complex and are shown in Figure 2. MEP surfaces are characterized by three colors, namely blue, red, and green which represent positive, negative, and neutral regions, respectively. In the DDQ (acceptor), the positive dark blue color region (0.0625 au) located on the phenyl ring switched to light blue (0.0451 au), and the negative regions which were located on the C=O and C≡N groups changed from -0.023 and -0.0403 au to -0.023 and -0.034 au, respectively. The donor (TEA) major negative

region (red) is located on the N atom (-0.0439 au) and decreased to 0.0246 au converting to a positive region upon complexation. The MEP results indicate that charge transfer takes place from donor to acceptor to form a stable CT complex.

3.2.3. Frontier molecular orbitals CT complex

The HOMO and LUMO electron density isosurfaces of the CT complex obtained from the DFT method are shown in Figure 3 and it is clear that the LUMO of the CT complex is mainly localized on the DDQ molecule, while the HOMO is situated on only TEA. When we observe the energy levels of HOMO and LUMO of TEA, DDQ, and CT complex, it is interesting to notify that, the HOMO energy of CT complex (-6.44 eV) is nearly close to the HOMO energy of TEA (-5.55 eV) and the LUMO energy of CT complex (-4.62 eV) is close to LUMO energy of DDQ (-5.09 eV). Therefore, the orbital interaction

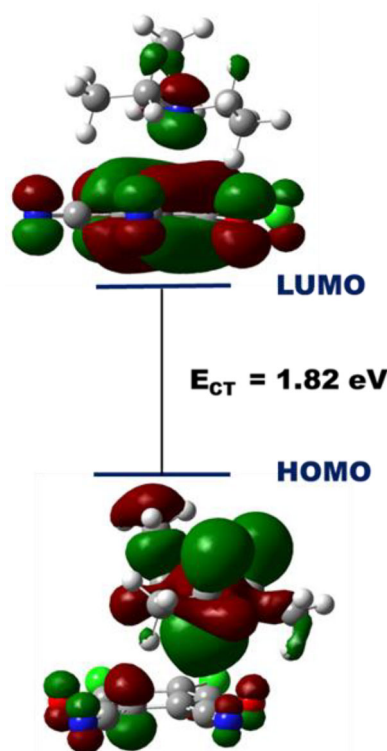


Figure 3. Electron density distribution in frontier molecular orbitals of CT complex.

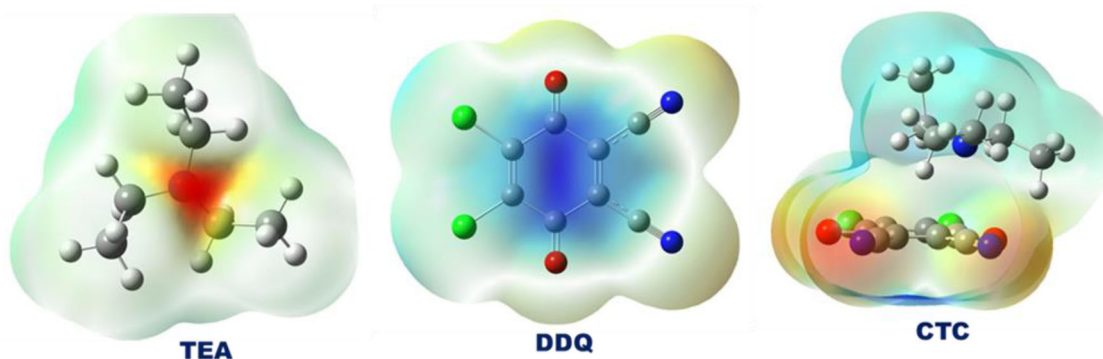


Figure 2. Molecular electrostatic potential surface maps of TEA, DDQ, and CTC complex.

energy mainly arises due to the charge transfer from the HOMO of TEA to the LUMO of DDQ which clearly indicates the formation of the CT complex.

3.3. Molecular descriptors calculated for QSAR modeling

In the present study, the antioxidant activity of fifteen chromones was considered for QSAR modeling. A total of thirteen molecular descriptors were calculated for each compound to correlate the antioxidant activity of the chromones (Tables S1 and S2). The antioxidant activity was calculated in the form of IC_{50} , it can be converted to PIC_{50} by using a formula $(-\log IC_{50})$. Finally, the multiple linear regression method was applied to develop the QSAR models and the resulting model has a high correlation coefficient (R) value. To validate the predictive potential of QSAR models, the leave-one-out cross-validation method was applied. Finally, the best model was obtained after the elimination of the B7 compound as an outlier, which increase in a square of correlation coefficient R^2 with acceptable predicted and residual values. As shown in Figure 4, the experimental

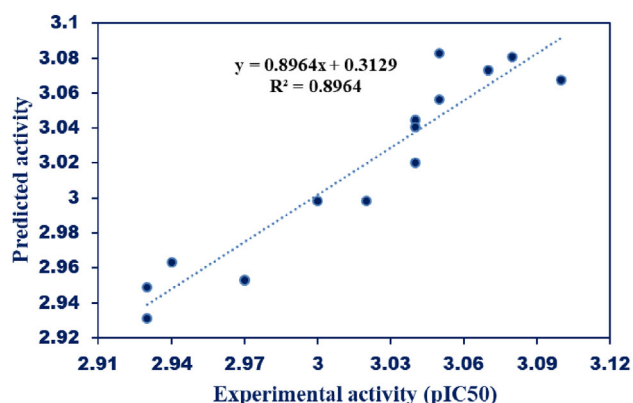


Figure 4. A plot between experimental antioxidant activity vs. predicted activity.

activity of the chromone derivatives was highly correlated with the predicted activity of the compounds.

$$\begin{aligned} \text{Activity} = & 2.378 \times 0.313 + 86.3 (\pm 25.1) * EA + 88.0 (\pm 25.2) * \eta \\ & + 0.588 (\pm 0.133) * \omega + 87.8 (\pm 25.1) * \mu \\ & + 0.069 (\pm 0.0194) * DM - 0.035 (\pm 0.006) \text{LogP} \end{aligned}$$

$R = 0.946$, $R^2 = 0.89$, $R^2_{\text{adj}} = 0.81$, $S.E = 0.024$, $F = 10.09$, Significance $F = 0.0037$, $S.D = 0.089$, $PRESS = 0.0041$, $Q^2_{\text{cv}} = 0.96$, $Q = 39.416$.

3.4. Molecular docking studies of celecoxib and ligands against COX2 enzyme

To develop the novel chromone compounds as antioxidant COX2 inhibitors, we performed the molecular docking studies of chromones against COX2 enzyme by using two well-validated docking programs GOLD and AutoDock. The most probable binding site and the active site residues of 4COX complexed with an inhibitor indomethacin (crystal structure bounded ligand) were identified by using Swiss PDB viewer 4.1.0 (Guex & Peitsch, 1997) software. The active site amino acids of 4COX such as ARG120, VAL349, LEU390, TYR355, TYR385, TRP387, MET522, VAL523, ALA527, and SER530 were involved in interactions with indomethacin. Recent research by Jones Lipinski et al. (2021) and Wang et al. (2010) reported that the molecular docking studies of celecoxib against 4COX have shown interactions with the active site residues ARG120 and TYR355. In order to understand the binding affinity and binding orientation of our molecules, we initially carried out the molecular docking analysis of a well-known drug and a selective inhibitor of COX2, i.e. celecoxib, and calculated the binding energy of -9.90 kcal/mol. As shown in Figure 5, the $-NH_2$ group of celecoxib has two hydrogen interactions with GLU524 and one C-H bond with ARG120 and other hydrophobic interactions with PRO84, VAL89, TYR155, VAL116, and

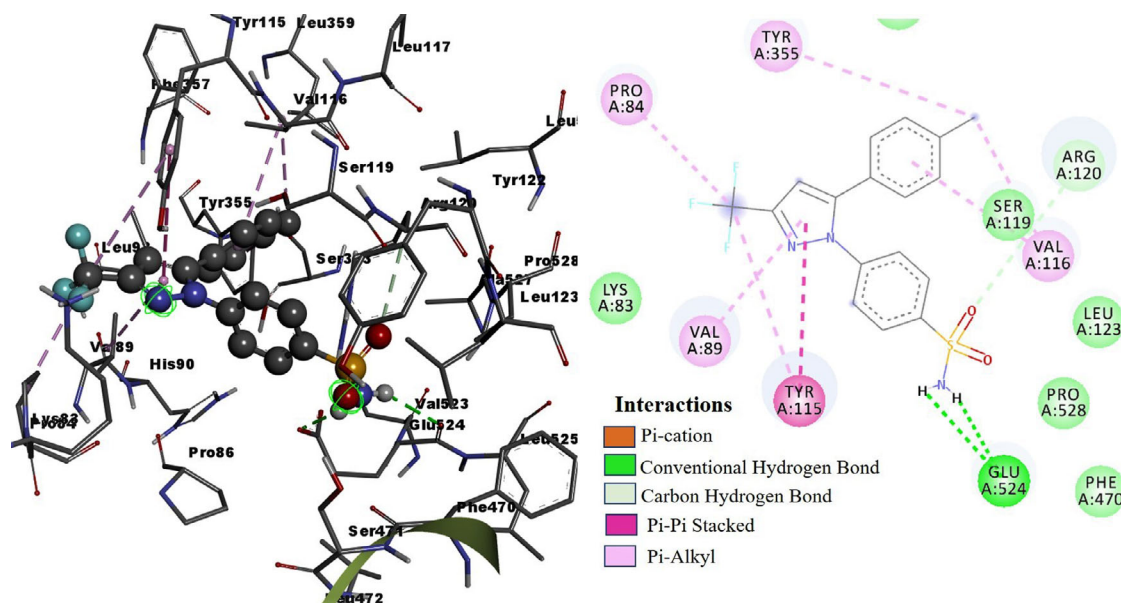


Figure 5. Binding orientation of celecoxib in the active site of COX2 (4COX). The left and right figures represent the molecular interactions of the ligand in 3D and 2D diagrams, respectively. The celecoxib is shown in the ball-stick model and active site residues are shown as grey sticks.

Table 2. The molecular docking results of chromone compounds with their inhibition constants.

Compounds	Binding energy (kcal/mol)	Chem-score	Fitness score	S(hb_ext)	S(vdw_ext)
B1	−9.17	32.03	60.14	1.59	49.50
B2	−8.78	32.42	61.96	7.02	47.90
B3	−9.02	32.51	73.87	9.96	51.94
B4	−9.59	16.01	14.46	0.04	59.68
B5	−8.90	34.96	65.93	9.58	46.68
B6	−9.32	28.31	58.69	7.25	44.80
B7	−9.26	31.71	58.93	0.07	48.98
B8	−8.36	28.37	68.93	8.34	53.49
B9	−9.01	30.43	61.33	2.81	50.06
B10	−8.42	28.26	59.50	3.08	48.05
B11	−9.66	32.86	69.81	2.00	57.20
B12	−9.87	31.88	66.14	2.01	54.90
B13	−4.35	33.65	68.30	1.99	59.18
B14	−4.51	32.13	62.19	1.44	56.29
B15	−4.49	27.66	73.73	2.70	56.97
celecoxib	−9.90	30.86	67.50	1.34	57.95
Ascorbic acid	−4.59	32.64	59.71	6.25	46.09

S (hb_ext) protein-ligand hydrogen bond scores, S (Vdw_ext) protein-ligand van der Waals scores.

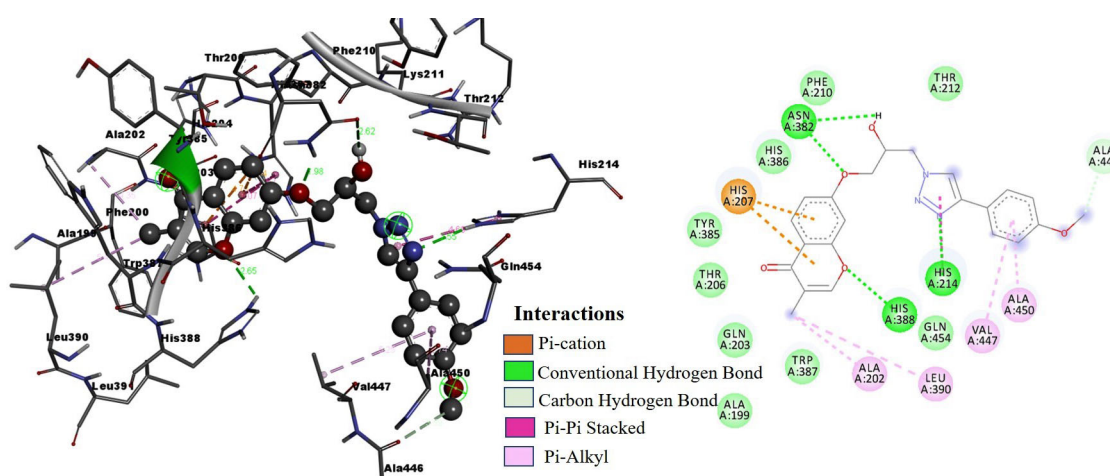


Figure 6. Binding orientation of compound B3 in the active site of COX2 (4COX). The left and right figures represent the molecular interactions of the ligand in 3D and 2D diagrams, respectively. The ligand B3 is shown in the ball-stick model and active site residues are shown as grey sticks. The interaction distances (Å) are shown in the 3D diagram.

TYR355. Our docking results also revealed the interactions of celecoxib with active site residues ARG120 and TYR355 of 4COX. Therefore, our molecular docking results are well-validated with previously published articles. Then, we calculated the binding energies, fitness scores, and chem scores for novel chromone compounds (Table 2). As per the GOLD docking results, the fitness and chem scores of the chromone compounds are between 14.46–73.87 and 16.01–34.96, respectively. Among the fifteen compounds, B3 and B8 compounds are the best antioxidants as well as anti-inflammatory COX2 inhibitors.

3.4.1. Binding modes of B3 and B8 compounds in the active site of COX2

The predicted binding mode of the active chromone compound B3 is shown in Figure 6. A 2D diagram of the B3 compound shows many interactions, such as hydrogen bonds, π - π T-shaped, alkyl, π -alkyl, π -cation, and C-H bond with active site residues of COX2. The inhibitory activity of B3 towards COX2 can be explained by these four hydrogen bond interactions with the active site residues such as HIS214, ASN382, and HIS388. Hydrogen bond interactions or the hydrophilic nature of compounds play a crucial role in inhibitory activity. From

GOLD results, it is clear that compound B3 has a high fitness score (73.87) and maximum external hydrogen bond score (9.96) than the other compounds. The binding energy (−9.02 kcal/mol) and chem-score value (32.51) also support the inhibitory activity of compound B3. The compound B3 also formed C-H bond interaction, π -cation, π - π T-shaped, alkyl, and π -alkyl interactions with ALA446, HIS207, HIS214, ALA202, LEU390, VAL447, and ALA 450.

The binding structure of compound B8 within the active site of COX2 is shown in Figure 7. It has formed two hydrogen bond interactions with HIS386 and HIS388 and one C-H bond interaction with TRP387. The residue HIS207 is involved in π -cation and π - π T-shaped interactions with chromone moiety. The other residues ALA202, HIS388, LEU390, and VAL447 are involved in π -alkyl interactions with chromone compounds. As per the docking results, compound B8 has a fitness score and chem score of 68.93 and 28.37, respectively.

3.5. Molecular dynamic simulations of COX2-ligand complexes

The MD simulations were carried out for three protein-ligand complexes of celecoxib (known drug of COX2), B3, and B8



compounds using Desmond with default protocols. The lowest binding energy conformations of protein-ligand complexes obtained from molecular docking were considered for MD simulations to evaluate the system's stability under solvent conditions. The final trajectory files are considered to calculate the 'root mean square deviation' (RMSD), and 'root mean square fluctuations' (RMSF) of the protein-ligand complexes.

The RMSD plot of celecoxib-COX2 is shown in [Figure 8\(a\)](#). The COX2 alpha chain (blue) RMSD value is increased to 2.06 Å with respect to its initial position at 1.89 ns, then decreased to 1.78 Å at 3.02 ns, and then increases again to 2.29 Å at 8.42 ns. The celecoxib-COX2 system was gradually tending to equilibrium after 9 ns and the average RMSD value is around 2.30 Å. During the simulation, such values represent the most suitable structural reconstruction. In the RMSD plot, 'Lig fit Prot' (maroon trajectory) shows the RMSD of a ligand with respect to the COX2 backbone and indicates how stable the ligand is in the protein active site.

ligand have shown an RMSF value of less than 2.0\AA that indicates, the catalytic site was stable during the simulation.

In addition, we investigated protein-ligand contact simulation results to validate the docking scores and binding energies. The figure shows the number of contacts with each residue and the type of interactions between residue and ligand such as hydrogen bonds, hydrophobic interactions, ionic interactions, and water bridges. The histogram plot in [Figure 10](#) shows the COX2-celecoxib contact and the dominant contribution to this interaction is from the residue GLU524, where, the H-bond and water bridge interactions form 0.62 and 0.54 interaction fractions (62% and 54% of the simulation time), respectively. The residues LEU80, PRO84, VAL89, LEU93, and TYR115 showed only hydrophobic interactions with the ligand. The residues PHE470 and SER471 have formed an H-bond interaction as well as a water bridge interaction with the ligand. In addition, as shown in [Figures 10](#) and S1, MD simulation determined new C-H bond interactions of residues LYS83 and PRO84 and a combination of other interactions with residues TYR122 (H-bond, hydrophobic, and water bridge), ARG120, and LEU123 (H-bond, hydrophobic, and water bridge), ARG469 (water bridge), PHE470 (H-bond and water bridge), and SER471 (H-bond and water bridge) which played an important role for the stabilization of celecoxib in the active site of COX2.

As shown in [Figure 8\(b\)](#), the COX2 alpha chain (blue) RMSD fluctuated initially and increased up to 3.20 ns with a value of 2.15 Å with respect to its initial position, then decreased to 1.81 Å at 5.75 ns after that the system inclined to equilibrium. The ligand RMSD with respect to protein fluctuated up to 18 ns after that it attained a stable energy position. The RMSD of the ligand is always lower than the RMSD of protein which indicates the ligand was stabilized in the active site during the simulation period. In the RMSF plot ([Figure 9b](#)), the major fluctuation was observed in the backbone at residue LEU80 with a value of 4.40 Å and the catalytic residues which were interacted with the ligand have shown low

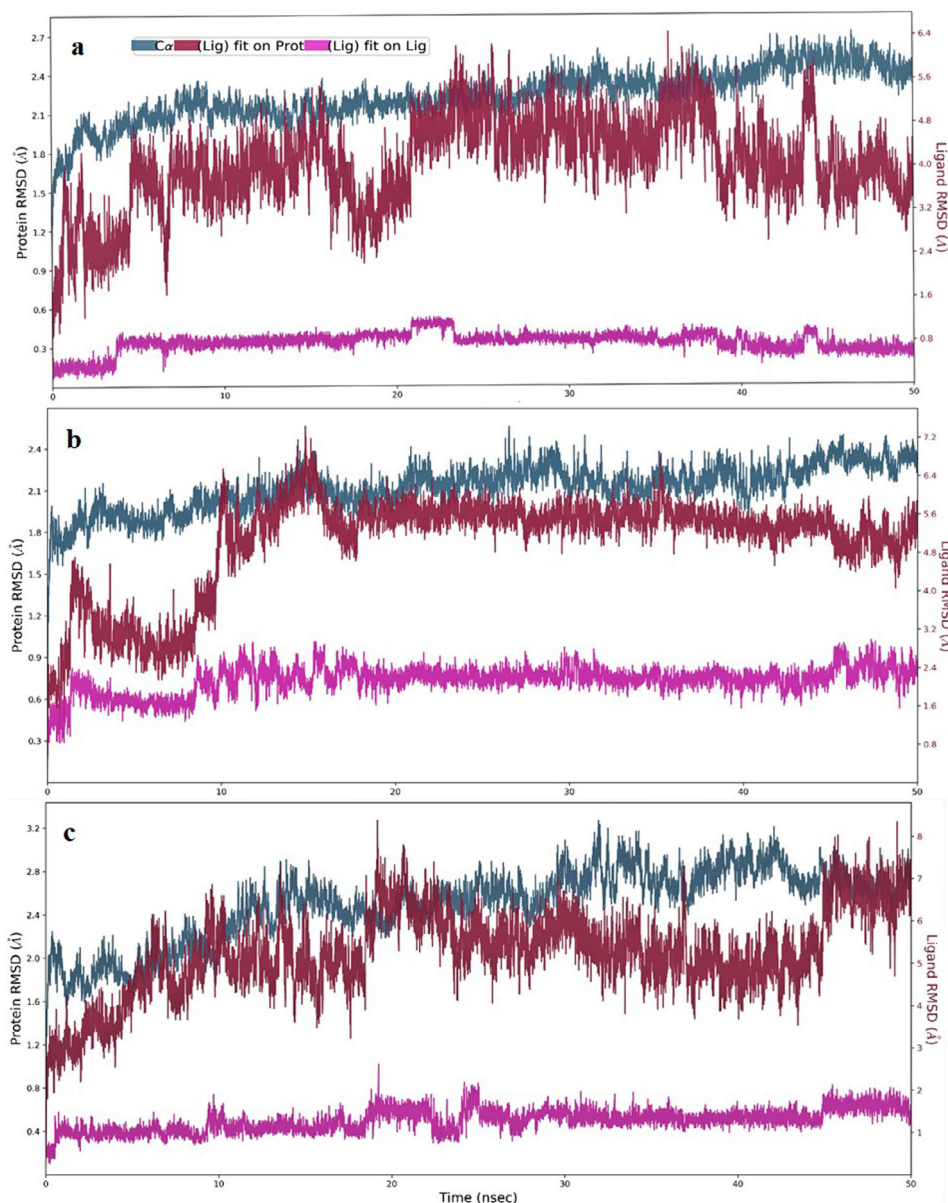


Figure 8. The RMSD plot of the celecoxib-COX2 complex with respect to the initial complex during 50 ns of MD simulation. (a) Celecoxib, (b) B3 compound, and (c) B8 compound. Blue, maroon, and pink color trajectories represent the RMSD evolution of the COX2 alpha chain, a ligand with respect to protein, and ligand with respect to the starting ligand, respectively.

RMSF values between 0.5–0.7 Å. The active site residues ALA199 (0.65 Å), GLN203 (0.55 Å), TYR385 (0.52 Å), and TYR386 (0.57 Å) were shown low RMSF values which means their fluctuations in the active site were very less and they have formed stable interactions with ligand during the simulation period. We calculated the RMSF plot (Figure 11) of the B3 ligand to understand the fluctuations of the ligand with respect to protein and internal fluctuations of the ligand with respect to the initial position of the ligand. In the RMSF plot, the fluctuation peaks were observed at atoms number 2 (2.80 Å), 9 (3.47 Å), 12 (2.76 Å), 29 (2.80 Å), and 30 (3.01 Å). These atoms are moving apart from the protein surface.

The MD simulations of the B3-COX2 complex (Figures 12 and S2) have shown different interactions like H-bond interactions, hydrophobic interactions, ionic interactions, and water bridges with the residues ALA199, GLN203, THR212, ASN382, TYR385, HIS386, TRP387, and VAL447. As shown in the histogram plot (Figure 12), 59% of the simulation time

ALA199 residue is involved in strong H-bond interaction followed by a water bridge with B3 ligand. The residues GLN203 and THR212 are involved in H-bond and water bridge interactions with a simulation time of 54%, and 37% respectively. The residues TYR385, HIS386, and TRP387 are involved in H-bond, hydrophobic, and water bridge interactions with a simulation time of 42%, 57%, and 49%, respectively. During the simulation, 2–8 residues of COX2 were interacting with the ligand.

The RMSD and RMSF plots of the B8-COX2 complex are given in Figures 8(c) and 9(c). According to Figure 8(c), the RMSD variations were observed up to 10 ns after that the system underwent equilibrium and the ligand was stabilized in the active site during the simulation. The RMSF plot of COX2 has shown that the fluctuations in residues were less than 3 Å which was an acceptable value. The fluctuations in the ligand concerning with protein active site were less than 2.3 Å, and therefore the ligand was stable in the active site

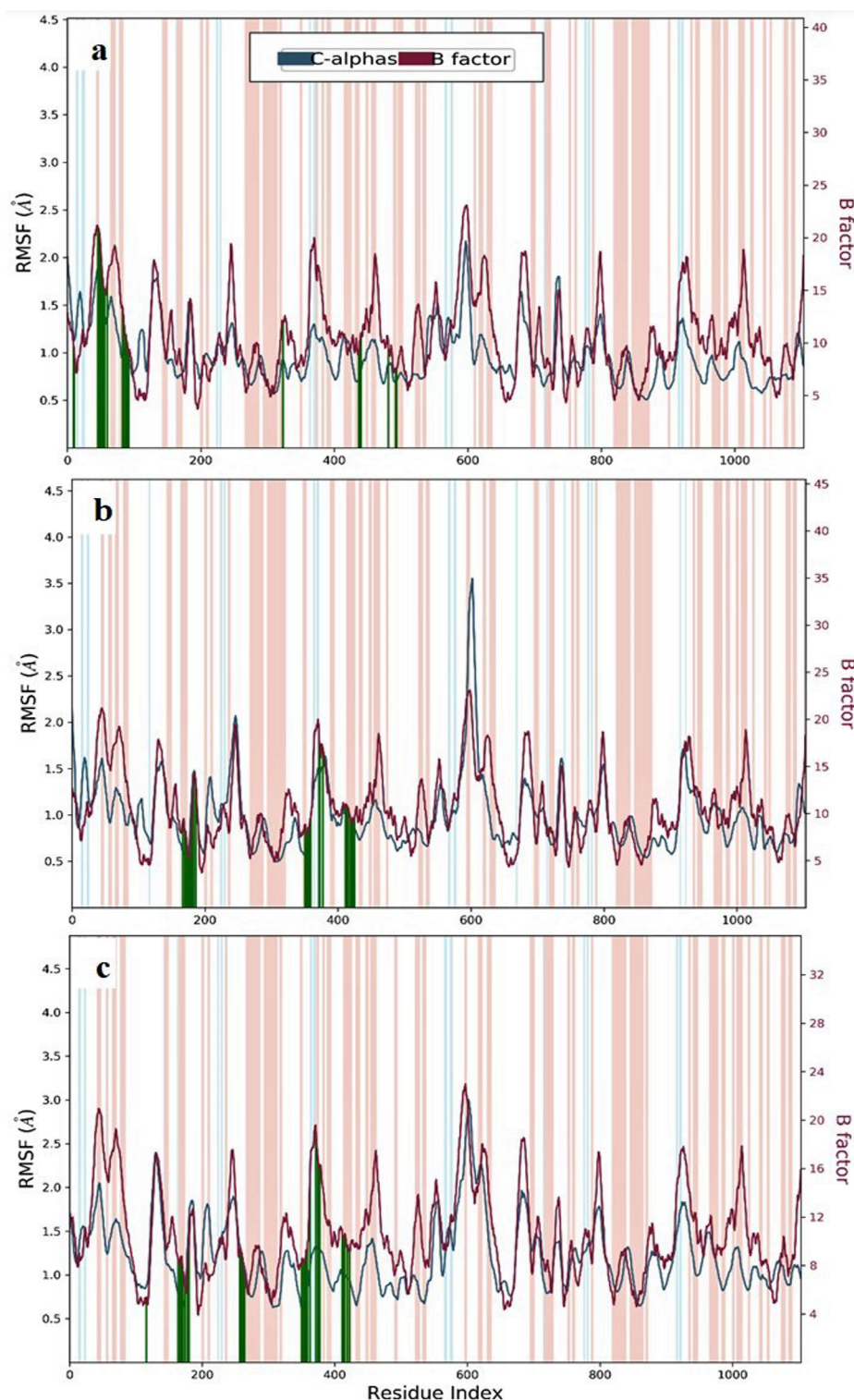


Figure 9. The RMSF plot of the celecoxib-COX2 complex concerning the initial complex during 50 ns of MD simulation. (a) Celecoxib, (b) B3 compound, and (c) B8 compound. Blue and maroon color trajectories represent the RMSF evolution of the COX2 alpha chain and experimental X-ray B-factor, respectively. Green color vertical bars represent the COX2 residues interacting with ligands.

pocket. According to the RMSF plot (Figure 13), during the simulation atoms number 5, 10, and 25 fluctuated more with respect to protein at the active site. Protein-ligand interaction diagrams (Figures 14 and S3) were established stable water bridge, H-bond, and hydrophobic interactions with active site residues such as GLN203, THR206, HIS207, ASN382, TYR385, and HIS388, and other residues were also

involved in interactions with less interaction fraction of less than 0.2.

3.6. Discussions

UV-Visible spectra of the donor ($\text{TEA} \sim 5 \times 10^{-4} \text{ M}$), acceptor ($\text{DDQ} \sim 5 \times 10^{-4} \text{ M}$), and CT complex are presented in Figure 15.

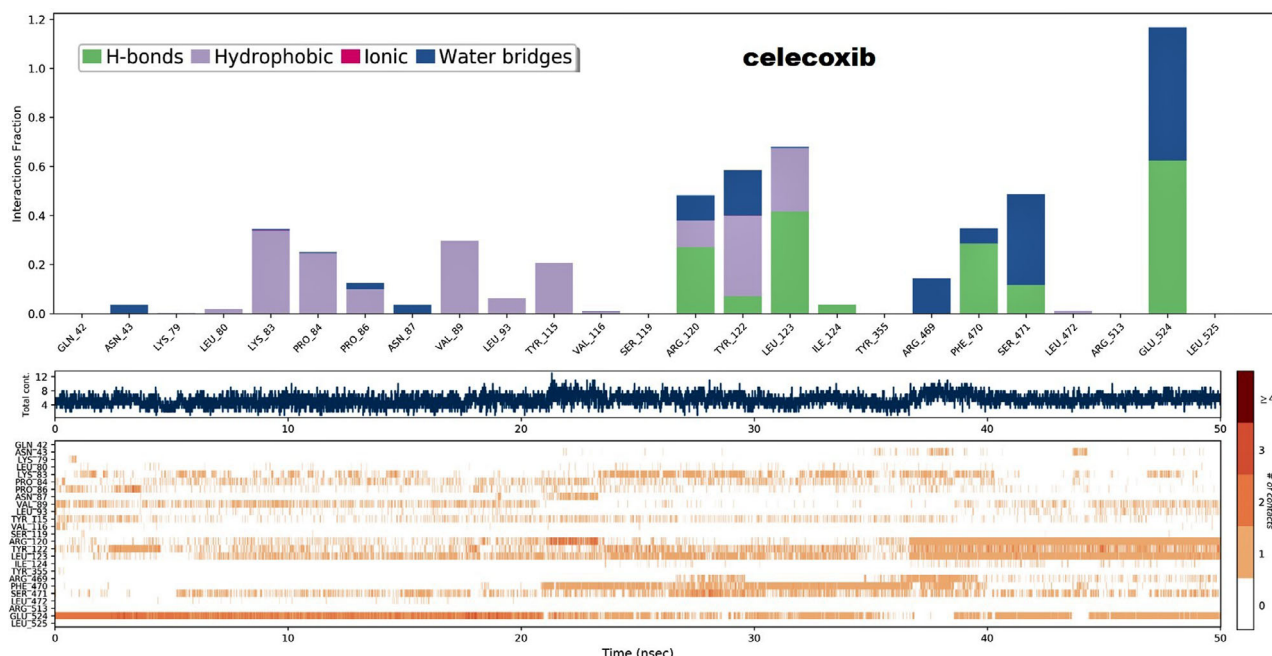


Figure 10. The histogram plot shows the interactions (H-bond, hydrophobic, ionic, and water bridge) of COX2 residues with the celecoxib. The blue trajectory shows the total number of specific contacts the COX2 makes with the ligand during the simulation time. The bottom panel shows which residues interact with the ligand in each trajectory frame.

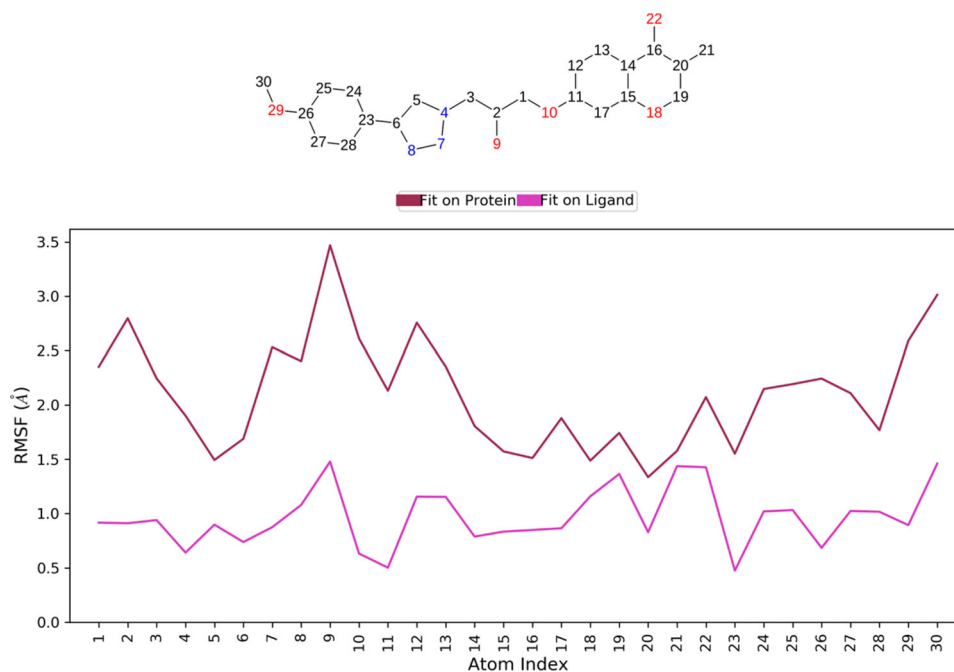


Figure 11. The RMSF plot of B3 ligand during 50 ns of MD simulation period.

The recorded spectrum shows factual charge transfer bands at 586, 547, and 450 nm, which did not exist in both free TEA and DDQ electronic absorption spectra. The CT-complex bands indicate the flow of electrons from donor to acceptor i.e. from closely located HOMO of TEA to LUMO of DDQ in the ground state. Moreover, it was detected as a red-brown color by mixing the acceptor and donor at low concentrations, which is considered an indication of CT complex formation.

The positive inductive effect of ethyl groups around N-atom in TEA and the high electron affinity of DDQ (~1.9 eV)

represent the donating and accepting natures of TEA and DDQ, respectively, were responsible for the generation of the radical ion pair. This is the trait of the radical ion pair resulting from the electron flow of TEA-N towards DDQ (quinone moiety) (Scheme 1). The solvent acetonitrile (polar) is utilized for the determination of the charge shift reaction between TEA and DDQ. The appearance of new absorption bands of the complex is stable for more than one hour at room temperature (298 K) in the acetonitrile medium. Then, we calculated the free radical scavenging activity of the chromone

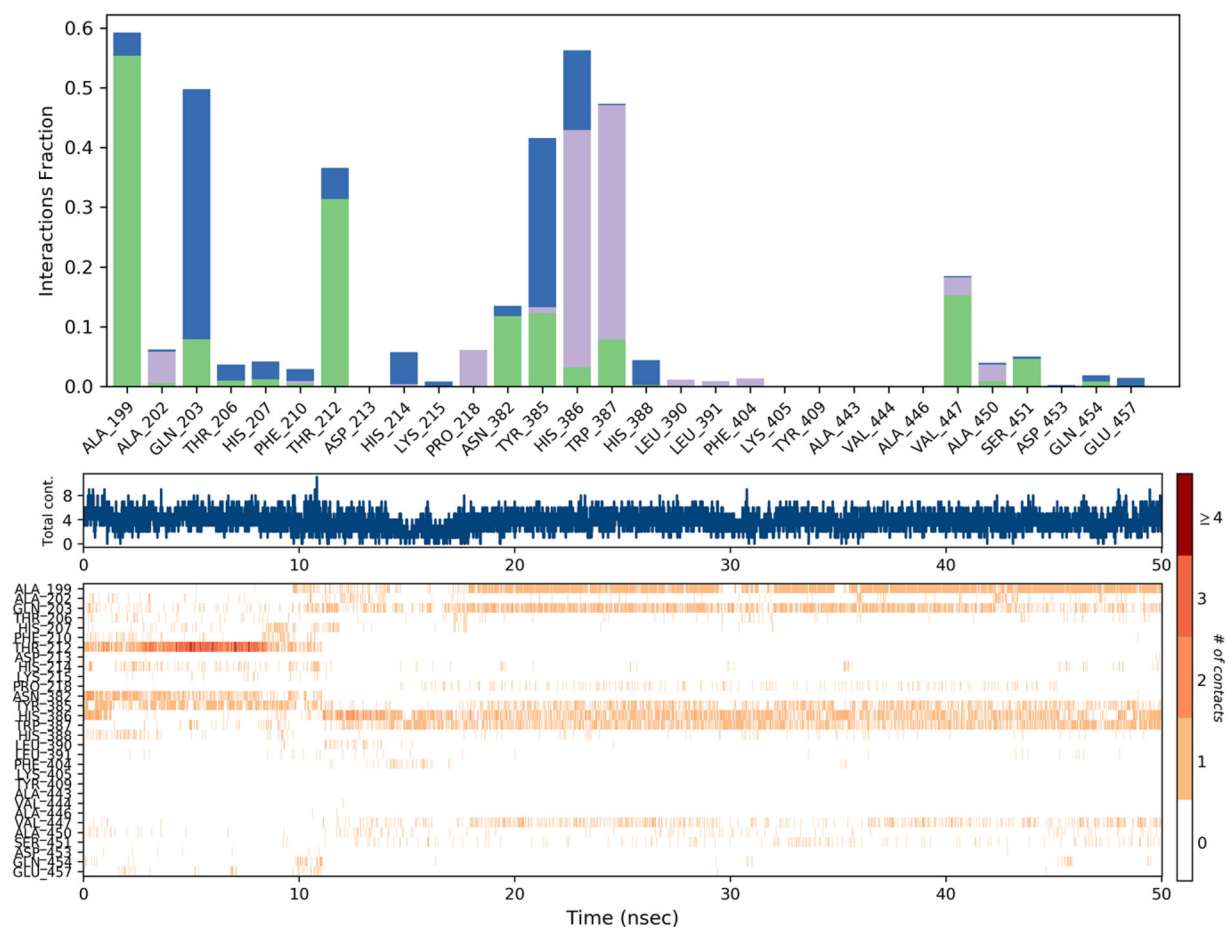


Figure 12. The histogram plot shows the interactions (H-bond, hydrophobic, and water bridge) of COX2 residues with the B3 ligand. The blue trajectory shows the total number of specific contacts the COX2 makes with the ligand during the simulation time. The bottom panel shows which residues interact with the ligand in each trajectory frame.

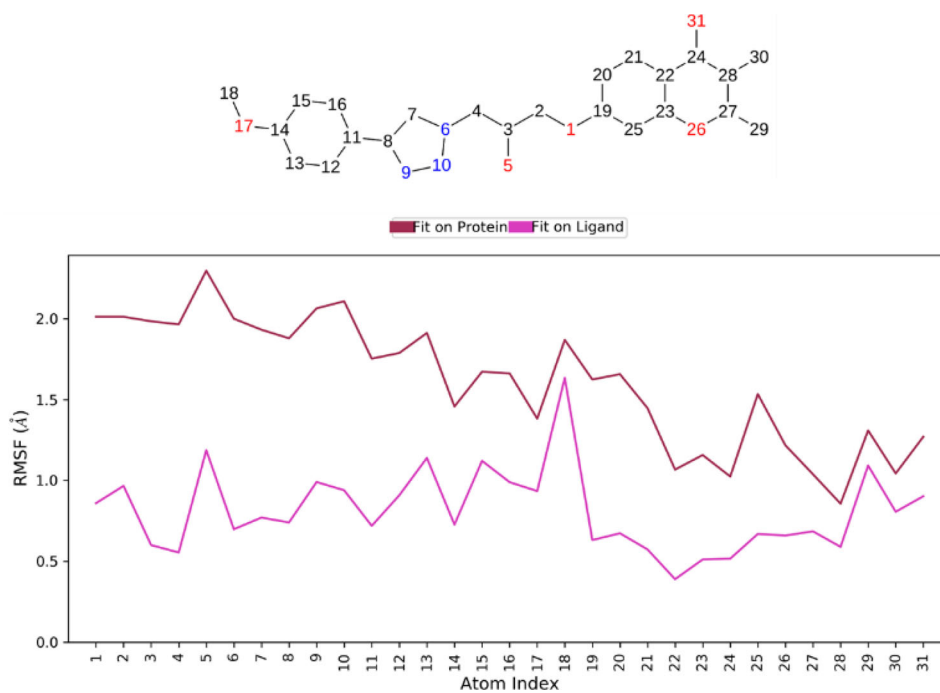


Figure 13. The RMSF plot of B8 ligand during 50 ns of MD simulation period.

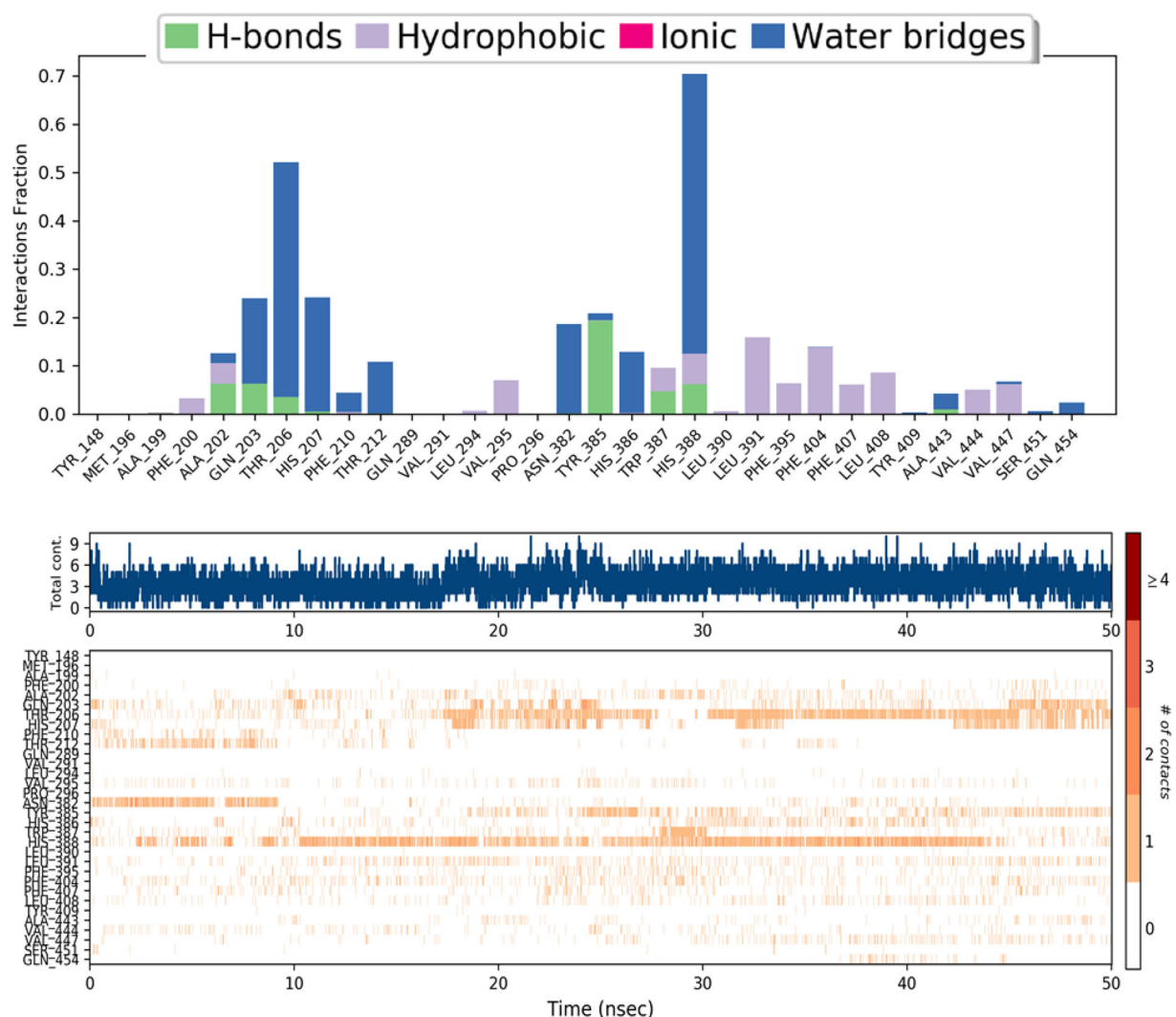


Figure 14. The histogram plot shows the interactions (H-bond, hydrophobic, and water bridge) of COX2 residues with the B8 ligand. The blue trajectory shows the total number of specific contacts the COX2 makes with the ligand during the simulation time. The bottom panel shows which residues interact with the ligand in each trajectory frame.

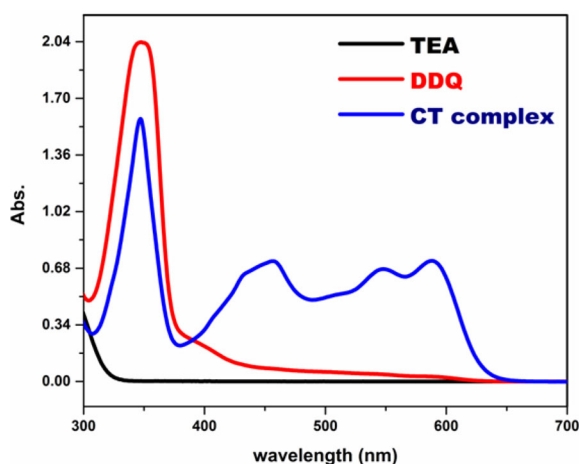


Figure 15. Observation of CT complex band from UV-Visible absorption spectra.

compounds against the DDQ assay. The CT complex formation was successfully explained by DFT calculations using MEPs and HOMO-LUMO isodensity plots.

In the present study, we developed a QSAR model for 15 chromone derivatives by considering various physiochemical parameters. The multiple linear regression method was applied by taking the antioxidant activity of the compounds as the dependent variable and all the calculated parameters as independent variables. The resulting QSAR model displayed a high correlation coefficient. Six molecular descriptors such as EA, hardness, electrophilic index, LogP, DM, and chemical potential were significantly correlated with the antioxidant activity of chromones. It is evident from the QSAR model that among the descriptors, EA, hardness, electrophilic index, DM, and chemical potential are positively correlated, which means the antioxidant activity increases when the values of these descriptors increase. On the other hand, the parameter LogP is negatively correlated with their antioxidant activity, which means activity increases when the values of these parameter decrease.

To explore the inhibitory activity of chromones, we performed molecular docking studies against the COX2 enzyme. GOLD software was utilized to calculate the fitness scores and chem scores of the molecules, and the binding energies

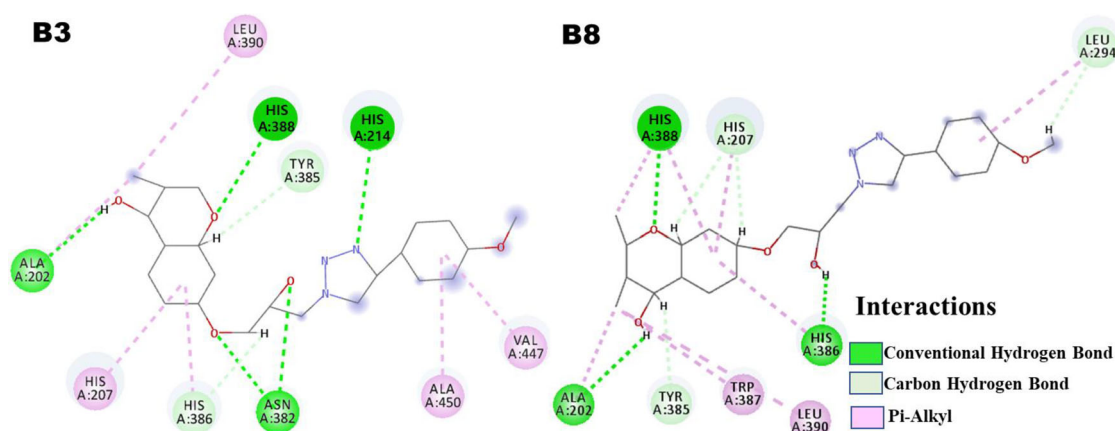


Figure 16. The conformational changes in the molecular structures of B3 and B8 during the MD simulation.

were calculated from AutoDock tools. To validate our results, first, we performed molecular docking of celecoxib (COX2 inhibitor) and calculated its binding energy. The ligand celecoxib was prepared by adding Gasteiger charges and 5 maximum number of torsions. The grid coordinates are defined as center_x = 22.332 Å; center_y = 26.138 Å and center_z = 13.373 Å; these grid coordinates are considered for further docking studies.

From molecular docking, we have identified the binding modes of our chromone derivatives in the active site of COX2. Further, we investigated the stability of docked complexes by calculating the RMSD, RMSF, and protein-ligand contact simulations using the MD simulations. The RMSD and RMSF plots of B3-COX2 and B8-COX2 complexes revealed that the complexes were stable throughout the simulation time. The results of protein-ligand contact simulations revealed key interactions of ligands with COX2. Interestingly, the MD simulation of B3-COX2 revealed new H-bond, Hydrophobic, and water bridge interactions with the residues ALA199, GLN203, THR212, TYR385, HIS386, and TRP387, and these interactions were maintained over the simulation with a considerable amount of time (Figures 12 and S2). The residues TYR385 and TRP387 are the most critical residues in permitting the cyclooxygenase to convert arachidonic acid (AA) to prostaglandins. A tyrosyl radical produced by TYR385 is crucial to initiate the rate-limiting step of cyclooxygenase catalysis, abstraction of 13-pro-S-hydrogen from AA (Thuresson et al., 2001); TRP387 residue forms a stable interaction with C-11 of arachidonic acid, resulting in an efficient endoperoxide synthesis. The residue His386 is positioned in the extended helix of PGHS (MEFNQNLHWHPL; 378–390), which contains two important residues, TYR385 cyclooxygenase active site residue, and the other HIS388, the proximal ligand to the heme group. HIS386 is more important for maintaining the structure of the unique extended helix of cyclooxygenase involving residues and it is in turn, necessary for optimizing heme and the resultant peroxidase and cyclooxygenase activities (Seibold et al., 2003; Smith & Song, 2002). Hydrogen bonding between heme propionate groups and amino acid side chains is another important mechanism for binding heme to

proteins. By eliminating this type of hydrogen bond, heme's binding strength to proteins gradually decreases (Poulos et al., 1997). In PGHSs, THR212 H-bonds through its backbone nitrogen and its side chain oxygen to the carboxylate oxygen of the D-ring propionate. ASN382 also hydrogen bonds to one of the oxygen of the D-ring propionates. Thus, the extended helix structure and robust propionate hydrogen bonding provide factors stabilizing the heme to compensate for weaker iron/His interactions (Thuresson et al., 2001). Also, the molecular docking and MD simulations of B8-COX2 revealed the interactions with these critical residues (TYR385, HIS386, ASN382, THR212, and HIS388) which are playing a key role in cyclooxygenase and peroxidase activities.

In addition, during the MD simulation relaxation steps, before the solvation of the protein-ligand complex, the system was allowed to relax for 12 ps. After relaxation, as shown in Figure 16, we observed the conformational changes in the molecular structure and new bonds formation of ligands B3 and B8 with the active site residues. The compound B3 formed a new C-H bond with TYR385 which facilitates the abstraction of Hydrogen from the B3 compound, Hydrophobic interaction with HIS386 and LEU390, and H-bond with ALA202. HIS207 is involved in π -cation interaction in the docking that has changed to π -alkyl interaction. These interactions are also observed after the completion of 50 ns of MD simulation time. Also, the B8 ligand established a C-H bond with TYR385 and LEU294, π -cation interaction of HIS207 has changed to two C-H bonds. Finally, based on our observations from molecular docking and dynamics the compounds B3 and B8 interacted with the key residues which were essential for cyclooxygenase and peroxidase catalytic reactions. Therefore, the molecules B3 and B8 are proposed as the best antioxidant and COX2 inhibitors.

4. Conclusions

In conclusion, we have estimated the free radical scavenging activity of fifteen novel chromone derivatives by using of DDQ assay method. This method utilizes the CT complex formation concept which is obtained by the chemical interaction between the electron donor and acceptor. The CT

complex formation was discussed with theoretical DFT calculations by considering MEPs and HOMO-LUMO isodensity surface plots. We have successfully derived the QSAR model to correlate the experimental antioxidant activity with the molecular descriptors of the chromone compounds and displayed a high correlation coefficient value. The QSAR model helps to estimate the antioxidant activity of newly designed chromone compounds from their molecular descriptors. In continuation, molecular docking studies of celecoxib and chromones were carried out to understand the inhibitory activity of the chromone compounds. Based on molecular docking results, the compounds B3 and B8 are found to be the best inhibitors of COX2. Further, we performed MD simulations of celecoxib, B3, and B8 ligands with COX2 complexes to explore the stability of the complexes by calculating the RMSD and RMSF plots. The three complexes are stable throughout the simulation time and no significant fluctuations were observed. Our compounds, B3 and B8 have strong interactions with the key amino acids (ASN382, TYR385, HIS386, TRP387, and HIS388) in the binding site. The *in vitro* bioassay reveals the compounds B3 and B8 have high free radical scavenging activity, whereas, the molecular docking and MD simulations confirm that these compounds are strong inhibitors of COX2.

Acknowledgments

The author, AL, expressed her gratitude to the Head, Department of Chemistry, Osmania University, Hyderabad, Bhavan's Vivekananda College of Science, Humanities & Commerce, Sainikpuri, Secunderabad. The authors thank Dr. Sampath Kumar Bandari and Dr. Nagaiah Kommu, Organic & Biomolecular Chemistry Division, CSIR-Indian Institute of Chemical Technology, Hyderabad, India for providing the chromone compounds in research work.

Disclosure statement

The authors declare that the research was conducted in the absence of any commercial or financial relationships that could be construed as a potential conflict of interest.

Funding

This study was funded by the National Research Foundation of Korea (NRF) grant funded by the Korean Government (2022R111A1A01071131).

Data availability statement

Data are contained within the article or [supplementary materials](#).

Authors' contributions

Conceived and designed the experiments: AL, SV, PT, and JJ; Performed the experiments: AL, NV; QSAR: AL and SV; Molecular docking and MD simulations: SV, JK, KK; Analyzed data: PT, AL; DFT: SV, NV; Contributed reagents/materials/analysis tools: PT, JJ; Writing-Original draft preparation: PT, JJ, AL, and SV; Writing-Review and editing: AL, SV, NV; Supervision: PT, JJ.

References

- Alam, M. N., Bristi, N. J., & Rafiquzzaman, M. (2013). Review on *in vivo* and *in vitro* methods evaluation of antioxidant activity. *Saudi Pharmaceutical Journal: SPJ: The Official Publication of the Saudi Pharmaceutical Society*, 21(2), 143–152. <https://doi.org/10.1016/j.jsps.2012.05.002>
- Amira, I. S., Yara, E. M., Mohamed, A. A., Omnia, A., Zainab, M. K., Ahmed, M. S., Samar, S. F., & Rania, H. A. H. (2022). Novel pyrrolopyrimidine derivatives: design, synthesis, molecular docking, molecular simulations and biological evaluations as antioxidant and anti-inflammatory agents. *Journal of Enzyme Inhibition and Medicinal Chemistry*, 37(1), 1821–1837. <https://doi.org/10.1080/14756366.2022.2090546>
- Arunapriya, L., Naveen, B., & Parthasarathy, T. (2017). Synthesis, spectroscopic and computational studies of charge-transfer complexation between 4-aminoaniline and 2,3-dichloro-5,6-dicyano-1,4-benzoquinone. *Journal of Solution Chemistry*, 46, 2171–2190. <https://doi.org/10.1007/s10953-017-0685-9>
- Bandari, S. K., & Kommu, N. (2016). *Novel synthesis of chromone, indole, Imidazo[1,2- α] pyridine and quinoxaline based hybrid heterocyclics as potential bioactive agents* (Unpublished doctoral thesis). Organic & Biomolecular Chemistry Division, CSIR-Indian Institute of Chemical Technology, Hyderabad, India.
- Bandari, S. K., Kammari, B. R., Madda, J., Kommu, N., Lakkadi, A., Vuppala, S., & Tigulla, P. (2017). Synthesis of new chromeno-carbamodithioate derivatives and preliminary evaluation of their antioxidant activity and molecular docking studies. *Bioorganic & Medicinal Chemistry Letters*, 27(5), 1256–1260. <https://doi.org/10.1016/j.bmcl.2017.01.047>
- Becke, A. (1993). Density-functional thermochemistry. III. The role of exact exchange. *The Journal of Chemical Physics*, 98(7), 5648–5652. <https://doi.org/10.1063/1.464913>
- Becke, A. D. (1996). Density-functional thermochemistry. IV. A new dynamical correlation functional and implications for exact-exchange mixing. *Journal of Chemical Physics*, 104(3), 1040–1046. <https://doi.org/10.1063/1.470829>
- Bergdorf, M., Robinson-Mosher, A., Guo, X., Law, K.-H., Shaw, D. E., & Shaw, D. E. (2021). *Research, Tech. Rep.* DESRES/TR–2021-01.
- Bowers, K. J., Chow, E., Xu, H., Dror, R. O., Eastwood, M. P., Gregersen, B. A., Klepeis, J. L., Kolossvary, I., Moraes, M. A., & Sacerdoti, F. D. Scalable algorithms for molecular dynamics simulations on commodity clusters; Proceedings of the 2006 ACM/IEEE Conference on Supercomputing, Tampa, FL, USA, 11–17 November 2006 84-es.
- Brame, E. G., & Dekker, M. (1972). *Applied Spectroscopy Reviews*, 17, 1–149.
- De Vries, E. F. J. (2006). Imaging of cyclooxygenase-2 (COX-2) expression: Potential use in diagnosis and drug evaluation. *Current Pharmaceutical Design*, 12, 3847–3856. <http://dx.doi.org/10.2174/138161206778559650>
- Foster, R. (1969). *Organic charge transfer complexes* (Vol. 51, p. 387). Academic Press.
- Frisch, M. J., Trucks, G. W., Schlegel, H. B., Scuseria, G. E., Robb, M. A., Cheeseman, J. R., Scalmani, G., Barone, V., Petersson, G. A., Nakatsuji, H. et al. (2016). Gaussian 16, Revision B.01. Wallingford, CT, USA.: Gaussian, Inc.
- Fu, J. Y., Masferrer, J., Seibert, K., Raz, A., & Needleman, P. (1990). The induction and suppression of prostaglandin H2 synthase (cyclooxygenase) in human monocytes. *The Journal of Biological Chemistry*, 265(28), 16737–16740. [https://doi.org/10.1016/S0021-9258\(17\)44821-6](https://doi.org/10.1016/S0021-9258(17)44821-6)
- Gamal-Eldeen, A. M., Djemgou, P. C., Tchuendem, M., Ngadjui, B. T., Tane, P., & Toshifumi, H. (2007). Anti-cancer and immunostimulatory activity of chromones and other constituents from *Cassia petersiana*. *Zeitschrift Fur Naturforschung. C, Journal of Biosciences*, 62(5–6), 331–338. <https://doi.org/10.1515/znc-2007-5-622>
- Gautam, R., Karkhile, K. V., Bhutani, K. K., & Jachak, S. M. (2010). Anti-inflammatory, cyclooxygenase (COX)-2, COX-1 inhibitory, and free radical scavenging effects of *Rumex nepalensis*. *Planta Medica*, 76(14), 1564–1569. <https://doi.org/10.1055/s-0030-1249779>
- Guex, N., & Peitsch, M. C. (1997). SWISS-MODEL and the Swiss-PdbViewer: An environment for comparative protein modeling. *electrophoresis*, 18(15), 2714–2723. <https://doi.org/10.1002/elps.1150181505>

- Halliwell, B., & Gutteridge, J. M. C. (2015). Free radicals in biology and medicine. Oxford University Press.
- Hawkey, C. J. (2005). COX-2 chronology. *Gut*, 54(11), 1509–1514. <https://doi.org/10.1136/gut.2005.065003>
- Jones Lipinski, R. A., Thillier, Y., Morisseau, C., Sebastiano, C. S., Smith, B. C., Jr., Hall, C. D., & Katritzky, A. R. (2021). Molecular docking-guided synthesis of NSAID-glucosamine bioconjugates and their evaluation as COX-1/COX-2 inhibitors with potentially reduced gastric toxicity. *Chemical Biology & Drug Design*, 98(1), 102–113. <https://doi.org/10.1111/cbdd.13855>
- Jones, G., Willett, P., Glen, R. C., Leach, A. R., & Taylor, R. (1997). Development and validation of a genetic algorithm for flexible docking. *Journal of Molecular Biology*, 267(3), 727–748. <https://doi.org/10.1006/jmbi.1996.0897>
- Kruk, I. (1997). Environmental toxicology and chemistry of oxygen species. Springer Science & Business Media.
- Kujubu, D. A., Fletcher, B. S., Varnum, B. C., Lim, R. W., & Herschman, H. R. (1991). TIS10, a phorbol ester tumor promoter-inducible mRNA from Swiss 3T3 cells, encodes a novel prostaglandin synthase/cyclooxygenase homologue. *The Journal of Biological Chemistry*, 266(20), 12866–12872. [https://doi.org/10.1016/S0021-9258\(18\)98774-0](https://doi.org/10.1016/S0021-9258(18)98774-0)
- Laube, M., Kniess, T., & Pietzsch, J. (2013). Radiolabeled COX-2 inhibitors for non-invasive visualization of COX-2 expression and activity—a critical update. *Molecules (Basel, Switzerland)*, 18(6), 6311–6355. <https://doi.org/10.3390/molecules18066311>
- Laube, M., Kniess, T., & Pietzsch, J. (2016). Development of antioxidant COX-2 inhibitors as radioprotective agents for radiation therapy—A hypothesis-driven review. *Antioxidants*, 5(2), 14. <https://doi.org/10.3390/antiox5020014>
- Marnett, L. J., Rowlinson, S. W., Goodwin, D. C., Kalgutkar, A. S., & Lanzo, C. A. (1999). Arachidonic acid oxygenation by COX-1 and COX-2. Mechanisms of catalysis and inhibition. *The Journal of Biological Chemistry*, 274(33), 22903–22906. <https://doi.org/10.1074/jbc.274.33.22903>
- Morris, G. M., Huey, R., & Olson, A. J. (2008). Using auto-dock for ligand-receptor docking. *Current protocols in bioinformatics* (Vol. 24, pp. 8.14. 1–8.14. 40). <https://doi.org/10.1002/0471250953.bi0814s24>
- Nampally, V., Palnati, M. K., Baidla, N., Varukolu, M., Gangadhari, S., & Tigulla, P. (2022). Charge transfer complex between O-Phenylenediamine and 2, 3-Dichloro-5, 6-Dicyano-1, 4-Benzoquinone: Synthesis, spectrophotometric, characterization, computational analysis, and its biological applications. *ACS Omega*, 7(19), 16689–16704. <https://doi.org/10.1021/acsomega.2c01177>
- Pizzino, G., Irrera, N., Cucinotta, M., Pallio, G., Mannino, F., Arcoraci, V., Squadrito, F., Altavilla, D., & Bitto, A. (2017). Oxidative stress: Harms and benefits for human health. *Oxidative Medicine and Cellular Longevity*, 2017, 8416763. <https://doi.org/10.1155/2017/8416763>
- Poulos, T. L., Hunter, C. L., Lloyd, E., Eltis, L. D., Rafferty, S. P., Lee, H., Smith, M., & Mauk, A. G. (1997). Role of the heme propionates in the interaction of heme with apomyoglobin and apocytochrome b5. *Biochemistry*, 36(5), 1010–1017. <https://doi.org/10.1021/bi961385u>
- Preeti, Y., Badri, P., Priyanka, M., & Sunil, Sharma, K. (2014). Chromones and their derivatives as radical scavengers: A remedy for cell impairment. *Current Topics in Medicinal Chemistry*, 14, 2552–2575.
- Rao, C., Bhat, S., & Dwedi, P. (1972). Spectroscopy of electron donor-acceptor systems. *Applied Spectroscopy Reviews*, 5(1), 1–170. <https://doi.org/10.1080/05704927208081699>
- Reis, J., Gaspar, A., Milhazes, N., & Borges, F. (2017). Chromone as a privileged scaffold in drug discovery: Recent advances. *Journal of Medicinal Chemistry*, 60(19), 7941–7957. <https://doi.org/10.1021/acs.jmedchem.6b01720>
- Salem, H. (2002). Spectrophotometric determination of beta-adrenergic blocking agents in pharmaceutical formulations. *Journal of Pharmaceutical and Biomedical Analysis*, 29(3), 527–538. [https://doi.org/10.1016/S0731-7085\(02\)00100-0](https://doi.org/10.1016/S0731-7085(02)00100-0)
- Seibold, S. A., Ball, T., Hsi, L. C., Mills, D. A., Abeyasinghe, R. D., Micielli, R., Rieke, C. J., Cukier, R. I., & Smith, W. L. (2003). Histidine 386 and its role in cyclooxygenase and peroxidase catalysis by prostaglandin-endoperoxide H synthases. *Journal of Biological Chemistry*, 278(46), 46163–46170. <https://doi.org/10.1074/jbc.M306319200>
- Smith, W. L., & Song, I. (2002). The enzymology of prostaglandin endoperoxide H synthases-1 and -2. *Prostaglandins & Other Lipid Mediators*, 68–69, 115–128. [https://doi.org/10.1016/S0090-6980\(02\)00025-4](https://doi.org/10.1016/S0090-6980(02)00025-4)
- Smith, W. L., DeWitt, D. L., & Garavito, R. M. (2000). Cyclooxygenases: Structural, cellular, and molecular biology. *Annual Review of Biochemistry*, 69(1), 145–182. <https://doi.org/10.1146/annurev.biochem.69.1.145>
- SPSS Software. (n.d.). Consult. <http://www.spss.com>
- Srimai, V., Ramesh, M., Satya Parameshwar, K., & Parthasarathy, T. (2013). Computer-aided design of selective Cytochrome P450 inhibitors and docking studies of alkyl resorcinol derivatives. *Medicinal Chemistry Research*, 22(11), 5314–5323. <https://doi.org/10.1007/s00044-013-0532-5>
- Termini, J. (2000). Hydroperoxide-induced DNA damage and mutations. *Mutation Research*, 450(1–2), 107–124. [https://doi.org/10.1016/S0027-5107\(00\)00019-1](https://doi.org/10.1016/S0027-5107(00)00019-1)
- Thuresson, E. D., Lakkides, K. M., Rieke, C. J., Sun, Y., Wingerd, B. A., Micielli, R., Mulichak, A. M., Malkowski, M. G., Garavito, R. M., & Smith, W. L. (2001). Prostaglandin endoperoxide H synthase-1: The functions of cyclooxygenase active site residues in the binding, positioning, and oxygenation of arachidonic acid. *The Journal of Biological Chemistry*, 276(13), 10347–10357. <https://doi.org/10.1074/jbc.M009377200>
- Valko, M., Leibfriz, D., Moncol, J., Cronin, M. T., Mazur, M., & Telser, J. (2007). Free radicals and antioxidants in normal physiological functions and human disease. *The International Journal of Biochemistry & Cell Biology*, 39(1), 44–84. <https://doi.org/10.1016/j.biocel.2006.07.001>
- Venkatesh, N., Naveen, B., Venugopal, A., Suresh, G., Mahipal, V., Manojkumar, P., & Parthasarathy, T. (2019). Donor-acceptor complex of 1-benzoylpiperazine with p-chloranil: Synthesis, spectroscopic, thermodynamic and computational DFT gas phase/PCM analysis. *Journal of Molecular Structure*, 1196, 462–477. <https://doi.org/10.1016/j.molstruc.2019.06.083>
- Wang, J. L., Limburg, D., Graneto, M. J., Springer, J., Hamper, J. R., Liao, S., Pawlitz, J. L., Kurumbail, R. G., Maziasz, T., Talley, J. J., Kiefer, J. R., & Carter, J. (2010). The novel benzopyran class of selective cyclooxygenase-2 inhibitors. Part 2: The second clinical candidate having a shorter and favorable human half-life. *Bioorganic & Medicinal Chemistry Letters*, 20(23), 7159–7163. <https://doi.org/10.1016/j.bmcl.2010.07.054>
- Xie, W., & Herschman, H. R. (1996). Transcriptional regulation of prostaglandin synthase 2 gene expression by platelet-derived growth factor and serum. *The Journal of Biological Chemistry*, 271(49), 31742–31748. <https://doi.org/10.1074/jbc.271.49.31742>
- Yagi, A., Kabash, A., Okamura, N., Haraguchi, H., Moustafa, S., & Khalifa, T. (2002). Antioxidant, free radical scavenging and anti-inflammatory effects of aloesin derivatives in Aloe vera. *Planta Medica*, 68(11), 957–960. <https://doi.org/10.1055/s-2002-35666>